

## Characterization of microcrystalline cellulose isolated through mechanochemical method

Norhafzan Junadi<sup>1</sup>, M D H Beg<sup>1,a</sup>, Rosli M Yunus<sup>1</sup>, Ridzuan Ramli<sup>2</sup>, Z A Zianor Azrina<sup>1</sup> & A K M Moshui Alam<sup>3</sup>

<sup>1</sup>Faculty of Chemical & Natural Resources Engineering, Universiti Malaysia Pahang,

Tun Razak Highway, 26300 Kuantan, Pahang, Malaysia

<sup>2</sup>Biomass Technology Unit, Malaysian Palm Oil Board, 6 Persiaran Institusi, Bandar Baru Bangi, 43000 Kajang, Selangor, Malaysia

<sup>3</sup>Institute of Radiation and Polymer Technology, Bangladesh Atomic Energy Commission, Bangladesh

Received 4 May 2017; revised received and accepted 27 November 2017

Mechanochemical process, which involves simultaneous ultrasound and alkali treatment, has been used to isolate microcrystalline cellulose (MCC) from raw oil palm empty fruit bunch (REFB) fibre. Three steps have been used to prepare the MCC, namely removal of lignin, removal of hemicellulose and finally production of MCC. The crystallinity index in MCC is found to be 81% which is 54% higher than that of REFB and 45% higher than that of cellulose. Besides crystallinity, the crystal size (28.03Å) of MCC is also enhanced noticeably by 53% as compared to the REFB and 28% as compared to cellulose. The degradation temperature, and the residue content reveal the excellent thermal stability of MCC extracted through this mechanochemical technique.

**Keywords:** Crystallinity index, *Elaeis guineensis*, Empty fruit bunch fibre, Mechanochemical process, Microcrystalline cellulose, Thermal stability

### 1 Introduction

Oil palm is an *Elaeis guineensis* species which is globally the utmost edible oil producing source. Annually, a huge amount of cellulosic oil palm biomass is generated from the palm oil mills. The cellulosic fibres can be extracted from different part of the palm tree, such as trunk, frond, fruit mesocarp and empty fruit bunch (EFB). Among all of these possible cellulose fibre sources, EFB is of particular interest. This is because EFB has the potential to give up to 73% cellulose, and it is expedient in terms of abundant availability and cost. In general, EFB fibre comprises about 42.7–65% cellulose, 13.2–25.31% lignin, 17.1–33.5% hemicellulose and 68.3–86.3% holocellulose<sup>1</sup>.

Cellulose is a renewable and biodegradable polymer which may be obtained from various plant sources. Naturally, cellulose molecules are biologically synthesized and assembled as microfibrils, which partially consist of crystalline and amorphous region<sup>2,3</sup>. It is widely used as the raw material in the production of cellulose acetate, rayon, cellophane and several other cellulose derivatives. It can be used for the production of films, sponge, food casing, fibres, membranes, paper and so forth<sup>4,6</sup>. Therefore, the demand for cellulose is

increase especially in application relating to renewable materials<sup>7,9</sup>.

Currently, researchers are paying more attention to the extraction of high quality microcrystalline cellulose (MCC) from different plant sources. It has great potential for use as an effective reinforcing agent especially in structural composites. Moreover, the MCC has wide applications in food, cosmetic and medical industries. The MCC can be extracted from different sources, using different approaches, which is the reason why MCC can exhibit different properties. The variation in MCC properties in terms of crystallinity, surface area, morphology structure, particle size as well as thermal stability depends on their raw material origin, treatment condition and the extraction process<sup>10</sup>. Several processes, such as acid hydrolysis<sup>11</sup>, pulp beating<sup>12</sup>, high pressure homogenizing<sup>13</sup> and cryocrushing<sup>14</sup>, have been used to extract MCC from different cellulosic materials.

Among the possible methods for MCC extraction, conventional acid hydrolysis method is very common<sup>14-16</sup>. However, report shows that this conventional isolation technique consumes a huge amount of corrosive acid and requires long processing time which makes it less technically desirable, in addition to the fact that it is not environment-friendly<sup>17</sup>. Hence, there is a need to obtain other alternative methods for MCC production. One possible approach is the use of

<sup>a</sup>Corresponding author.  
E-mail: dhbeg@yahoo.com

ultrasonic treatment, which can be incorporated to improve the hydrolysis method. At the moment, the use of ultrasonic-assisted hydrolysis method for production of MCC is not common. Therefore, this study has been designed to isolate microcrystalline cellulose using a mechanochemical method which involves simultaneously both ultrasonic process and alkali treatment. This method can be a potential alternative for acid hydrolysis because of less chemical consumption and retention time as well as low cost, and it is environment friendly<sup>18</sup>.

Ultrasonication is a way of creating combined physical and chemical effects within a system through the use of sound wave. It transfers energy during acoustic cavitation, which involves formation, growth and collapse of bubbles in a liquid<sup>19</sup>. Several studies have shown the potential application of ultrasonication as a pretreatment method for lignocellulosic biomass<sup>20-22</sup>, whereby it has been suitable for degrading polysaccharide linkages and disrupt polymers bond. However, it is worthy of note that the structural changes achieved after ultrasonic treatment can be the influencing factors, such as sonication power, temperature and treatment duration. On the other hand, ultrasonication has shown ability to facilitate hydrolysis by inducing molecular motion, mainly in macromolecule cell without altering the chemical composition of the lignocellulosic biomass<sup>23</sup>.

In this study, the ultrasonic-assisted alkali treatment approach to extract MCC is believed to be a potential alternative to the conventional acid hydrolysis method. The presence of alkali treatment will not only help in extracting the MCC, but it is also expected to increase the number of free reactive hydroxyl groups available on the fibre surface. This will provide valuable advantage to the MCC for different applications.

## 2 Materials and Methods

### 2.1 Materials

Raw empty fruit bunch (REFB) fibres were supplied by Malaysian Palm Oil Board (MPOB), Bangi, Malaysia. The chemicals used in this work were acetic acid ( $\text{CH}_3\text{COOH}$ ), sodium chlorite ( $\text{NaClO}_2$ ) and sodium hydroxide ( $\text{NaOH}$ ), purchased from Sigma-Aldrich (USA).

### 2.2 Methods

#### 2.2.1 Preparation of REFB Fibre

REFB was washed with hot deionized water (DI) ( $85 \pm 5^\circ\text{C}$ ) in order to remove non-structural impurities, such as sand, mud, stain, palm fruit, palm seed, seed grains and seed shell. Then, REFB was squeezed

manually to remove excess water and then allowed to dry in open air for 48 h. After drying, REFB fibre was ground using ECO grinder and sieved using a sieve shaker (Lab sieve shaker, LS 300T) in order to get uniform diameter at approximately  $400 \mu\text{m}$ .

#### 2.2.2 Delignification of REFB Fibre

The flow chart for the delignification process of REFB fibre is illustrated in Fig. 1. In an Erlenmeyer flask, the fresh ground REFB fibres were mixed into DI water at a ratio of 1:30. Then, 60 wt% sodium chlorite ( $\text{NaClO}_2$ ) and 60 wt% acetic acid with respect to dried REFB fibre were added into this solution. The slurry was thoroughly mixed by shaking the flask; the flask was incubated in a fume hood at  $70^\circ\text{C}$  with intermittent mixing up to 4 h. After the reaction was completed, the slurry was vacuum filtered in order to separate the liquid from the treated REFB fibre, identified as holocellulose. The holocellulose was washed repeatedly using DI water at  $25^\circ\text{C}$  until the solution gets yellow color and odor is disappeared and the pH value is approximately neutral. The white holocellulose was then dried in oven (Memmert UM 100) and subjected for subsequent treatment.

#### 2.2.3 Extraction of Cellulose

The flow chart for cellulose extraction process is presented in Fig. 1. Holocellulose was treated with 17.5%  $\text{NaOH}$  solution at  $20^\circ\text{C}$  for 2 h in order to dissolve the hemicellulose. After that, the slurry was vacuum filtered, and the insoluble cellulose mass was separated and again washed with 8.3%  $\text{NaOH}$  solution. A few drops of 10% acetic acid solution were added to neutralize the excess  $\text{NaOH}$  present in

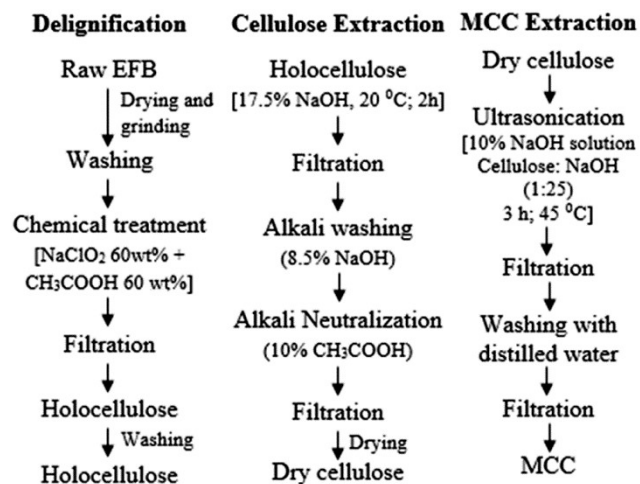


Fig. 1 — Delignification, cellulose extraction and MCC preparation processes

the cellulose slurry. Then, the cellulose obtained was vacuum filtered and dried in an oven at 105°C for 18 h and then subjected to characterization and subsequent treatment.

#### 2.2.4 Preparation of MCC

Figure 1 also illustrates the flow chart of MCC extraction process. The MCC was isolated from neat cellulose using the mechanochemical technique. The cellulose obtained as described in the previous section was soaked in 10 % NaOH solution in which the ratio of cellulose to alkali solution was 1:25. The suspension was then subjected to ultrasonic treatment in an ultrasound bath (Elma 37 kHz, power capacity 320 W, Germany) at 45 °C for 3 h. After that, the suspension was vacuum filtered and the MCC obtained was washed repeatedly with distilled water until it is free from alkali. The MCC was then dried in a vacuum oven at 105 °C until a constant weight was achieved. The dried MCC was milky-white in appearance. Finally, REFB fibre, cellulose and extracted MCC were subjected to different comparative characterization.

#### 2.2.5 FTIR Study

Fourier transform infrared spectroscopy (FTIR) was performed to observe the interaction behavior of functional groups in REFB, cellulose and MCC. The analysis was conducted using a Nicolet 6700 FTIR spectrometer, Thermo Scientific, Germany, following the standard KBr pellet technique. The FTIR spectra was obtained after 32 scans with a resolution of 4 cm<sup>-1</sup> and within the wave number range of 4000–500 cm<sup>-1</sup>.

#### 2.2.6 XRD Study

X-ray diffraction (XRD) was carried out to study the crystallinity of REFB, cellulose and MCC by using a Rigaku Mini Flex II, Japan, operated at 30 kV, 15 mA and equipped with computer to analyze the data. The samples were step-wise scanned in the range of scattering angle (2θ) from 3° to 40°, with a step of 0.02°, using CuK<sub>α</sub> radiation of wavelength λ=1.541Å. The data were recorded in terms of the diffracted X-ray intensities (I) versus 2θ.

#### 2.2.7 SEM Study

The morphology and size distribution of REFB, cellulose and MCC were observed by using Scanning Electron Microscope (SEM). The micrographs were taken by SEM-EDX Oxford INCA 400 model at an acceleration voltage of 15 kV. All samples observed were sputter coated with gold prior to SEM analysis.

#### 2.2.8 Thermogravimetric Analysis

Thermogravimetric analysis (TGA) was performed using TGA Q500 V6.4 (Germany) in a platinum crucible under a nitrogen gas atmosphere (flow rate 60 mL/min) with a heating rate of 10 °C/min. The scanning temperature range was 25 - 600 °C. Following Broide equation was applied to predict the kinetic parameters of REFB, cellulose and MCC<sup>24</sup>:

$$\ln \left[ \ln \frac{1}{x} \right] = -\frac{E_a}{RT} + \ln \left[ \frac{R\gamma}{E_a\beta} T_{(max)}^2 \right] \quad \dots (1)$$

where x is the fraction of non-volatilized material not yet decomposed; T<sub>max</sub>, the temperature of maximum reaction rate (°C); β, the heating rate (°C/min); γ, the frequency factor; E<sub>a</sub>, the activation energy (J/mol); and R, the gas constant (8.314 J/mol.K). Regression lines were drawn from the plots of lnln(1/x) versus 1/T using the data within the start and the end of TGA peak. Then, the value of E<sub>a</sub> for each sample was evaluated from the slope of the straight line.

### 3 Results and Discussion

#### 3.1 Interaction Mechanism

Figure 2 reveals the structural characteristics of cellulose and MCC isolated from REFB fibre. The absorption peaks characteristic and corresponding vibrational modes are represented in Table 1. The wide O-H stretching peak (3672-3002 cm<sup>-1</sup>) appears in the spectrum of REFB<sup>20, 25</sup>. The aliphatic C, H present in the natural fibre are attributed by the C-H bond stretching at 2918 cm<sup>-1</sup> and CH<sub>2</sub> bending vibration at 1394 cm<sup>-1</sup> (ref. 26). The absorption peak at 1730 cm<sup>-1</sup> is due to the presence of (>C=O) group in hemicellulose, which is present in REFB fibre. The

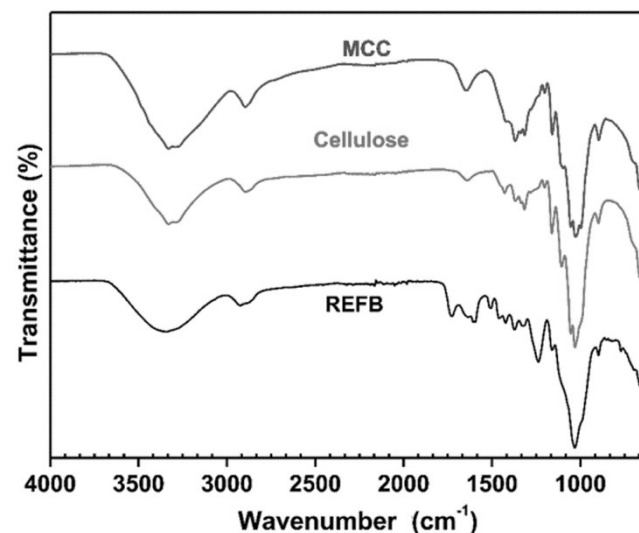


Fig. 2 — FTIR spectrum of REFB, cellulose and MCC

Table 1 — Characteristic transmittance peaks of REFB, cellulose and MCC

Sample	Wave number cm <sup>-1</sup>	Vibrational mode	
REFB	3372	H-bonded O-H stretching	
	2918	C-H stretching in alkane	
	1730	C=O stretching in ester of hemicellulose	
	1587-1503	C-C stretching, in benzene ring of lignin	
	1394	C-H bending and rocking in alkane	
	1231	C-O stretching in C-O-C aryl alkyl ether linkage in lignin segments	
	1033	C-O stretching, β-glucosidic linkage	
	897	Glycosidic bond	
	Cellulose	3341	H-bonded O-H stretching
		3338	O-H stretching of Intra molecular hydrogen bonding
3271		O-H stretching of intermolecular hydrogen bonding	
2887		C-H stretching in alkane	
1643		H-O-H stretching due to absorbed water	
1365-1317		C-H bending and rocking in alkane	
1023		C-O stretching, β-glucosidic linkage	
894		Glycosidic linkage	
MCC		3335	H-bonded O-H stretching
		3341	O-H stretching of Intra molecular hydrogen bonding
	3262	O-H stretching of intermolecular hydrogen bonding	
	2893	C-H stretching in alkane	
	1652	H-O-H stretching due to absorbed water	
	1364	C-H bending and rocking in alkane	
	1023	C-O stretching, β-glycosidic linkage	
	893	Glycosidic linkage	

absorption peaks at 1587-1503 cm<sup>-1</sup> indicates the C-C bond stretching of the benzene ring associated with lignin molecules in REFB fibre. Additionally, aryl-alkyl ether (-O-) linkage of lignin is obvious in the spectrum of REFB fibre; the corresponding peak of this functional group appears at 1231 cm<sup>-1</sup> (ref. 27). The relatively wide peak for glycosidic linkage of (-C-O) group in the cellulose molecule has appeared at 1033 cm<sup>-1</sup> as well.

In the spectrum of cellulose, the O-H stretching peak shifts towards the lower wave number, in the range of 3633-2983 cm<sup>-1</sup>. The shoulder like peaks appear at 3338 cm<sup>-1</sup> and 3271 cm<sup>-1</sup>; these peaks are associated with intramolecular hydrogen bonding and intermolecular hydrogen bonding in the cellulose

molecules respectively. The aliphatic C-H stretching peak has shifted towards the lower wave number as well. On the other hand, the carbonyl (>C=O) group peak corresponding to hemicellulose does not appear in the cellulose spectrum. Likewise, the functional group peaks corresponding to the lignin molecules are absent in the spectrum of cellulose. The absence of these characteristic peaks suggests that the lignin and hemicellulose are removed during the delignification process. The C-O stretching peak of the glucosidic linkage in cellulose molecule becomes narrow as compared to REFB peak and it appears at 1023 cm<sup>-1</sup>.

On the other hand, the O-H hydrogen bond stretching peak in the spectrum of MCC shifts towards the lower wavenumber in the range of 3675-2977 cm<sup>-1</sup>. The intra and intermolecular O-H hydrogen bond stretching appears at 3341 cm<sup>-1</sup> and 3262 cm<sup>-1</sup> respectively. The spectrum also illustrates the absence of lignin and hemicellulose molecules in the MCC. The C-O glucosidic linkage peak of MCC becomes sharper as compared to REFB and cellulose.

From the FTIR peaks (Fig. 2), it can be inferred that lignin and hemicellulose are completely removed from the MCC which might have led to increase density of O-H group on the surface of MCC. Therefore, this might have facilitated intramolecular and intermolecular hydrogen bonding within the MCC similar to the findings reported in literature<sup>28</sup>.

### 3.2 Morphological Analysis

Figure 3 illustrates the surface morphology of REFB (A), cellulose (B) and MCC (C) after isolation using ultrasound-assisted alkali treatment. The SEM micrographs show the distinguishable changes in the surface morphology of the fibres and MCC. The micrograph of REFB looks like a piece of timber, the surface is cemented with impurities which are responsible for producing cracks, and in addition, the fibre bundles are not obvious. On the other hand, cellulose micrograph (B) reveals smooth surface with a number of fibre bundles which indicates that cementing materials such as lignin, pectin, and hemicellulose have been eliminated from that timber like fibre surface<sup>15</sup>. Micrograph of MCC exhibits irregular shaped rough fibril surface. The size of MCC fibrils is narrow with most likely higher aspect ratio (L/D) as compared to cellulose fibres, similar morphology was also reported elsewhere<sup>29</sup>. This might be due to the depolymerization of the cellulose polymer chain<sup>30</sup> and possible particle breakage during the ultrasonic process assisted with alkali treatment<sup>20</sup>.

### 3.3 Structural Analysis

The X-Ray diffraction profiles of REFB, cellulose and MCC are illustrated in Fig. 4. The diffraction peaks of REFB appear at  $17.08^\circ$  and  $22.33^\circ$  with miller indices of (101) and (020) respectively. The peaks are basically diffused due to the presence of hemicellulose, lignin, pectin and other foreign impurities. However, in the cellulose diffractogram, the peaks appear at  $16.18^\circ$  and  $23.27^\circ$  with Miller

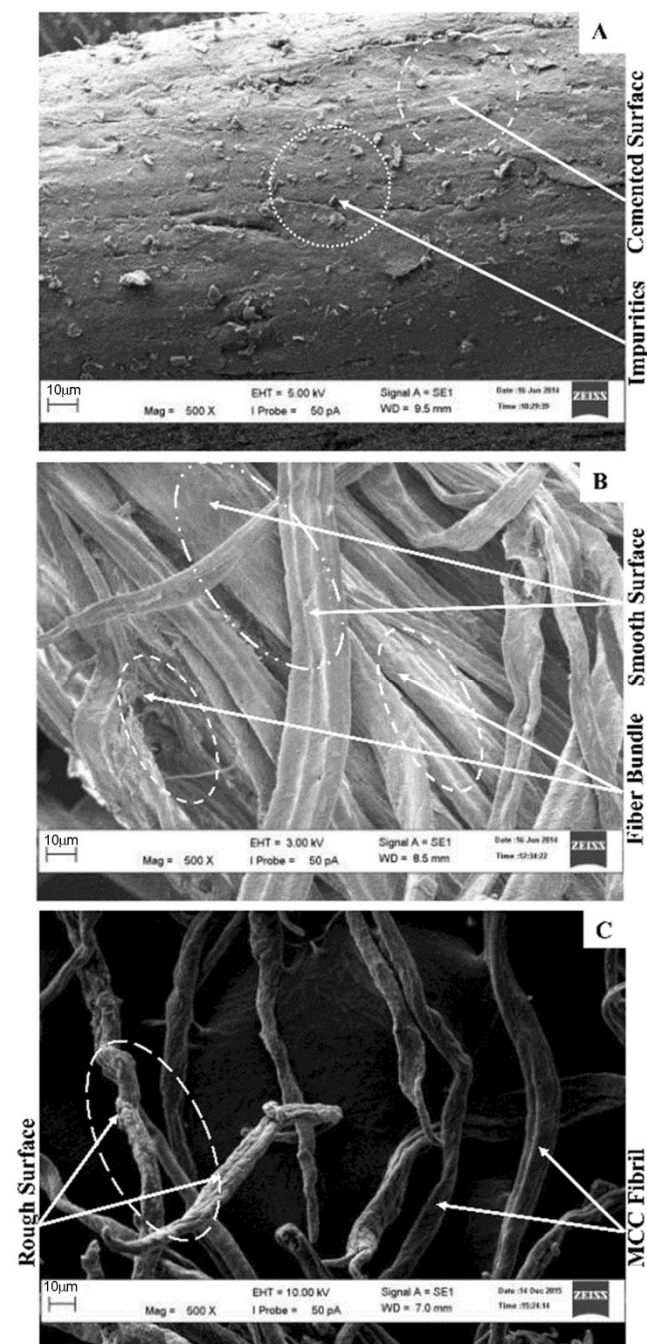


Fig. 3 — SEM micrographs of (A) REFB, (B) cellulose and (C) MCC

indices of (110) and (200) respectively which are less diffused as compared to REFB. The crystal region peak is shifted towards higher angle as well as the peak width is reduced due to the removal of noncellulosic compound from the REFB fibre. The diffractions peaks of MCC are shifted towards the highest angles at  $22.44^\circ$ ,  $28.57^\circ$  and  $34.51^\circ$  representing the Miller indices (002), (210) and (040) correspondingly<sup>30, 31</sup>. Additionally, the crystal plane (040) confirms the microcrystalline structure in the MCC. Thus, the molecules in MCC become ordered by simultaneous ultrasonic and alkali treatment of the intermediate cellulose material.

The calculated crystallinity index ( $\eta_{crys}$ ) and average crystal size (D) in the direction normal to the reflecting plane of REFB, cellulose and MCC are summarized in Table 2. The crystallinity index is calculated using the following equation:

$$\eta_{crys}\% = \frac{I_c}{I_c + I_A} \times 100 \quad \dots (2)$$

where  $I_c$  and  $I_A$  are the integrated intensities of crystal and amorphous parts of the samples respectively. The crystal size (D) is determined using the following Scherrer's equation<sup>32</sup>:

$$D = \frac{0.9\lambda}{\delta C \cos\theta} \quad \dots (3)$$

Table 2 — X-ray diffraction parameters of REFB, cellulose and MCC

Diffraction parameter	REFB	Cellulose	MCC
$\eta_{crys}, \%$	52.8	55.87	81
$D, \text{\AA}$	17.09	21.86	28.03

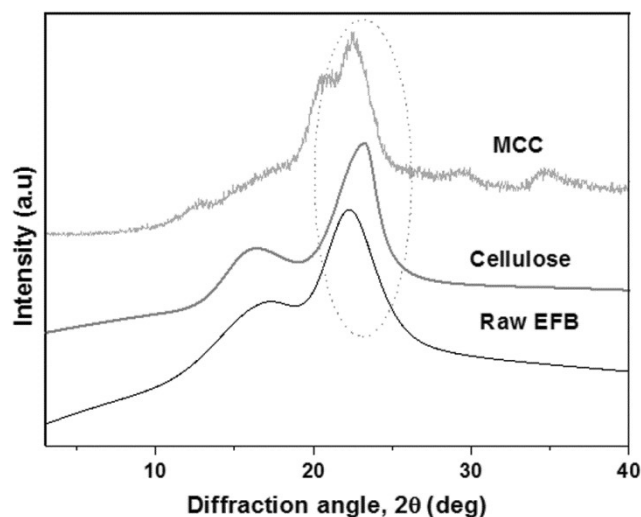


Fig. 4 — XRD profiles of REFB, cellulose and MCC

where  $\delta$  is the full width at half maximum (FWHM); and  $\lambda$  value is  $1.541 \text{ cm}^{-1}$ .

The crystallinity of MCC is increased by about 54% and 45% as compared to REFB and cellulose as intermediate material respectively. Therefore, ultrasound-assisted alkali treatment method potentially removes the chemical heterogeneity as well as improves the crystal perfection<sup>28, 33</sup>. Moreover, the crystal size of MCC is enhanced by 53% and 28% as compared to REFB and cellulose correspondingly.

### 3.4 Thermal Analysis

#### 3.4.1 Degradation

Figures 5(a) and (b) illustrate the TGA and DTG thermograms of cellulose and MCC derived from REFB fibre. In the TGA thermograms, the initial weight loss of REFB, cellulose and MCC are in the range of 30-125 °C due to the evaporation of adsorbed moisture on the surface of these materials<sup>34</sup>. Two steps decomposition is revealed in these

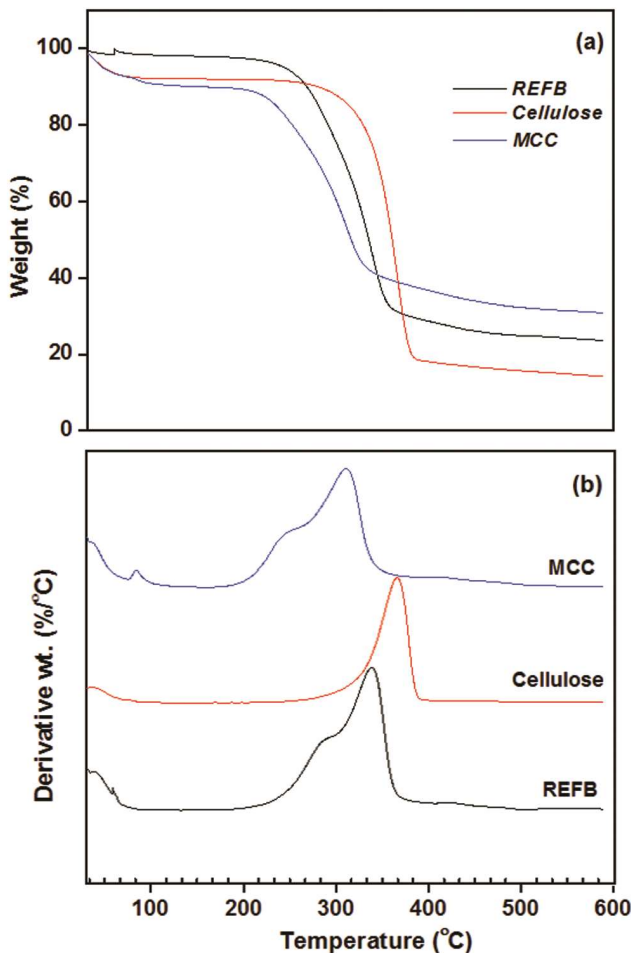


Fig. 5 — TGA (a), and DTG (b) thermograms of REFB, cellulose and MCC

thermograms; the corresponding decomposition temperature ranges of REFB, cellulose and MCC are 241-352 °C, 289-381 °C, and 219-327 °C respectively. The thermal degradation temperature of these materials are presented in Table 3, using the temperatures at 50% weight loss of the samples and the residue content at 600°C. The onset decomposition temperature and the temperature at which 50% degradation takes place for REFB and cellulose are higher than that for MCC.

The decomposition peak temperatures for all samples as obtained from the DTG thermograms which are designated as the  $T_{max}$  (°C) are summarized in Table 3. The key decomposition peak temperature of MCC is observed at 312 °C, whereas the decomposition peaks of REFB and cellulose occur at 340 °C and 367 °C respectively. These are considerable for degradation of cellulose as cellulosic materials, as stated elsewhere<sup>17</sup>. The decomposition of hemicelluloses starts below 400 °C followed by pyrolysis of lignin, depolymerization of cellulose, active flaming combustion and char oxidation<sup>35</sup>. The decomposition temperature ( $T_{50\%}$  and  $T_{max}$ ) of REFB and cellulose are higher as compared to MCC which is thought to be due to a drastic reduction in molecular weight of the MCC because of alkali treatment. It is also believed that alkali treatment of cellulose not only dissolves the amorphous regions but also disintegrates some crystalline regions<sup>36</sup>. However, it is noticeable that the weight loss of cellulose is 86% and that of MCC is 69%. The residue content of simultaneous ultrasound and alkali-treated MCC is 31%, which is higher than that of cellulose residue. This observation notices that crystal quality of simultaneous ultrasound-assisted alkali-treated MCC has better thermal stability as compared to the conventional process.

#### 3.4.2 Activation Energy Analysis

Figure 6 illustrates activation energy ( $E_a$ ), which have been calculated using Broido's plots for REFB, cellulose and MCC. The values of  $E_a$  obtained for REFB, cellulose and MCC are 29.36, 19.00 and 16.5

Table 3 — Thermal profiles of REFB, cellulose and MCC

Sample	Decomposition temperature ( $T_{50\%}$ ), °C	Residue content at 600 °C, wt%	DTG peak temperature ( $T_{max}$ ), °C
REFB	320	23.50	340
Cellulose	360	14	367
MCC	314	31	312

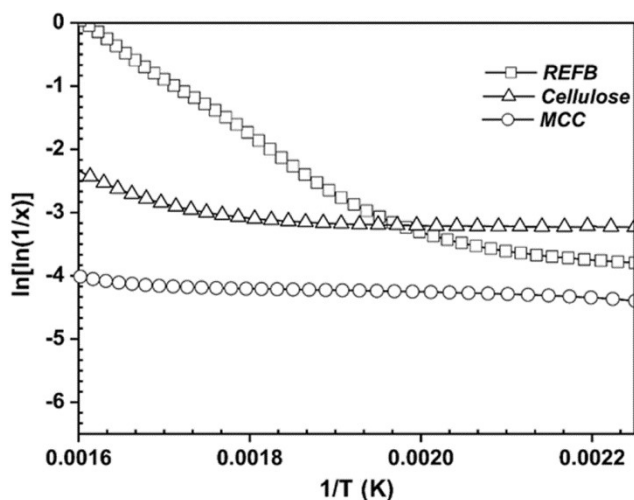


Fig. 6 — Broido's plots for REFB, cellulose and MCC for analysis of the activation energy

kJ/mol respectively. The  $E_a$  is known to represent the energy barrier preventing long chain molecules to move from one location to the other. Thus, the higher value of  $E_a$  represents the more thermal stability of a sample. Therefore, the observed results demonstrate that REFB and cellulose are thermally more stable than MCC. Similar observation is also reported for activation energy<sup>37</sup>.

#### 4 Conclusion

MCC has been isolated from REFB by using mechanochemical technique which involves pretreatment process followed by simultaneous ultrasound-assisted alkali treatment. The results obtained from interaction analysis reveal greater O-H group density on the surface of MCC which makes intra and intermolecular hydrogen bonds more feasible. Morphological analysis reveals that timber like REFB fibre structure is altered to become individual narrow fibres as a result of removal of the cementing materials. Microstructural analysis confirms the Miller indices of (040) in MCC, in addition to the narrow peak of crystal region which appears in the diffractogram of MCC. Additionally, MCC crystal size is increased as compared to the raw fibre. Moreover, the crystallinity index of MCC is higher as compared to REFB and cellulose fibre. The energy barrier for the molecular motion of cellulose in MCC is significantly decreased as compared to the raw materials. The temperature at 50% weight loss as well as residue content of MCC is noticeably higher as compared to the MCC obtained by conventional acid hydrolysis process. This observation indicates that MCC isolated by the mechanochemical

technique possess greater heat resistance properties compared to the conventional MCC.

#### Acknowledgement

The authors would like to thank Ministry of Education Malaysia for funding through FRGS/1/2018/TK05/UMP/01/2 and Malaysian Palm Oil Board (MPOB) for supporting through GSAS for this project.

#### References

- 1 Khalil H P S A, Siti M A, Ridzuan R, Kamarudin H & Khairul A, *Polym Plast Technol Eng*, 47 (2008) 273.
- 2 Brinchi L, Cotana F, Fortunati E & Kenny J M, *Carbohydr Polym*, 94 (2013) 154.
- 3 Nishiyama Y J, *Wood Sci*, 55 (2009) 241.
- 4 Inagaki T, Schwanninger M, Kato R, Kurata Y, Thanapase W, Puthson P & Tsuchikawa S, *Wood Sci Technol*, 46 (2012) 143.
- 5 Rodrigues B V M, Heikkilä E, Frollini E & Fardim P, *Cellulose*, 21 (2014) 1289.
- 6 Oliveira F B D, Bras J, Pimenta M T B, Curvelo A A S & Belgacem M N, *Ind Crops Prod*. <http://dx.doi.org/10.1016/j.indcrop.2016.04.064> (2016).
- 7 Hamzeh Y, Ashori A, Khorasani Z, Abdulkhani A & Abyaz A, *Ind Crops Prod*, 43 (2013) 365.
- 8 Chan W P, Won Y, Song Y H, Yong S K & Seung H L, *Wood Sci Technol*, doi:10.1007/s00226-016-0863-8 (2016).
- 9 Gan S, Shang H P, Hyoung J C, Sarani Z & Chin H C, *Carbohydr Polym*, 137 (2016) 693.
- 10 El-Sakhawy M & Hassan M L, *Carbohydr Polym*, 67 (2007) 1.
- 11 Haafiz M K M, Eichhorn S J, Azman H & Jawaid M, *Carbohydr Polym*, 93 (2013) 628.
- 12 Chakraborty A, Sain M & Kortschot M, *Holzforchung*, 59 (2005) 102.
- 13 Bruce D M, Hobson R N, Farrent J W & Hepworth D G, *Compos [Part A] Appl Sci Manuf*, 36 (2005) 1486.
- 14 Alemdar A & Sain M, *Bioresour Technol*, 99 (6) (2008) 1664.
- 15 Johar N, Ahmad I & Dufresne A, *Ind Crops Prod*, 37 (2012) 93.
- 16 Moran J I, Alvarez V A, Cyrus V P & Vazquez A, *Cellulose (Dordrecht, Netherlands)*, 15 (1) (2008) 149.
- 17 Jahan M S, Saeed A, He Z & Ni Y, *Cellulose*, 18 (2011) 451.
- 18 Klimakow M, Klobes P, Andreas F T, Klaus R & Franziska E, *Chem Mater*, 22(18) (2010) 5216.
- 19 Filson P B & Dawson-Andoh B E, *Bioresour Technol*, 100 (2009) 2259.
- 20 Alam A K M M, Beg M D H, Mina M F, Khan M R & Prasad D R M, *Compos Pt A*, 43 (2012) 1921.
- 21 Aimin T, Hongwei Z, Gang C, Guohui X & Wenzhi L, *Ultrason Sonochem*, 12 (2005) 467.
- 22 Ebringerová A & Hromádková Z, *Ultrason Sonochem*, 9 (2002) 225.
- 23 Huang R, Su R, Qi W & He Z, *Bioenergy Res*, 4 (2011) 225.
- 24 Broido A A, *J Polym Sci [Part A-2]*, 7 (1969) 1761.
- 25 Alam A K M, Mina M F, Beg M D H, Mamun A A, Bledzki A K & Shubhra Q T H, *Fiber Polym*, 15(6) (2014) 1303.
- 26 Ozlem I K, Cuneyt H U & Oya G A, *Carbohydr Polym*, 147 (2016) 37.

- 27 Olgun G, Sergio N M, Esperidiana A B M & Jaroslaw W D, *Polym Rev*, doi:10.1080/15583724.2016.1176037 (2016).
- 28 Xu X, Liu F, Jiang L, Zhu J Y, Darrin H & Dennis P W, *ACS Appl Mater Interfaces*, 5 (2013) 2999.
- 29 Mathew A P, Oksman K & Sain M, *J Appl Polym Sci*, 101 (2006) 300.
- 30 French A D, *Cellulose*, 21 (2014) 885.
- 31 French A D & Cintron M S, *Cellulose*, 20 (2013) 583.
- 32 Zhang W L, Liu Y D & Choi H J, *J Mater Chem*, 21 (2011) 6916.
- 33 Oudiani A E, Chaabouni Y, Msahli S & Sakli F, *Carbohydr Polym*, 86 (2011) 1221.
- 34 Rosa S M L, Rehman N, De M, Nachtigall M I G & Bica C I D, *Carbohydr Polym*, 87 (2012) 1131.
- 35 Jonoobi M, Khazaeian A, Md Tahir P, Azry S S & Oksman K, *Cellulose*, 18 (2011) 1085.
- 36 Mandal A & Chakrabarty D, *Carbohydr Polym*, 86 (2011) 1291.
- 37 Alvarez V A & Vázquez A, *Polym Degrad Stab*, 84(1) (2004) 13.